nature biomedical engineering

ARTICLES

https://doi.org/10.1038/s41551-022-00916-z

Check for updates

A wearable electrochemical biosensor for the monitoring of metabolites and nutrients

Minqiang Wang[1,7], Yiran Yang[1,7], Jihong Min[1,7], Yu Song[1], Jiaobing Tu[1], Daniel Mukasa[2], Cui Ye[1], Changhao Xu[1], Nicole Heflin[3], Jeannine S. McCune[4], Tzung K. Hsiai[5], Zhaoping Li[6] and Wei Gao[1]✉

Wearable non-invasive biosensors for the continuous monitoring of metabolites in sweat can detect a few analytes at sufficiently high concentrations, typically during vigorous exercise so as to generate sufficient quantity of the biofluid. Here we report the design and performance of a wearable electrochemical biosensor for the continuous analysis, in sweat during physical exercise and at rest, of trace levels of multiple metabolites and nutrients, including all essential amino acids and vitamins. The biosensor consists of graphene electrodes that can be repeatedly regenerated in situ, functionalized with metabolite-specific antibody-like molecularly imprinted polymers and redox-active reporter nanoparticles, and integrated with modules for iontophoresis-based sweat induction, microfluidic sweat sampling, signal processing and calibration, and wireless communication. In volunteers, the biosensor enabled the real-time monitoring of the intake of amino acids and their levels during physical exercise, as well as the assessment of the risk of metabolic syndrome (by correlating amino acid levels in serum and sweat). The monitoring of metabolites for the early identification of abnormal health conditions could facilitate applications in precision nutrition.

Circulating nutrients are essential indicators for overall health and body function[1]. Amino acids (AAs), sourced from dietary intake and gut microbiota synthesis, and influenced by personal lifestyles, are important biomarkers for a number of health conditions (Fig. 1a)[2]. Elevated branched-chain amino acids (BCAAs), including leucine (Leu), isoleucine (Ile) and valine (Val), are associated with obesity, insulin resistance and future risk of type 2 diabetes mellitus (T2DM), cardiovascular diseases (CVDs) and pancreatic cancer[3–5]. Deficiencies in AAs (for example, arginine and cysteine) could hamper the immune system by reducing immune-cell activation[6]. Tryptophan (Trp), tyrosine (Tyr) and phenylalanine (Phe) are precursors of serotonin and catecholamine neurotransmitters (dopamine, norepinephrine and epinephrine), respectively, and play an important role in the function of complex neural systems and mental health[7,8]. A number of metabolic fingerprints (including Leu, Phe and vitamin D) are linked to coronavirus disease 2019 (COVID-19) severity[9,10]. Health disparities in nutrition also correlate well with the alarming racial and ethnic disparities that are worsened by COVID-19 vulnerability and mortality[11]. Moreover, organ and tissue dysfunction induced by severe acute respiratory syndrome coronavirus 2 could result in an increased incidence of cardiometabolic diseases[12].

Metabolic profiling and monitoring are a key approach to enabling precision nutrition and precision medicine[13]. Current gold standards in medical evaluation and metabolic testing heavily rely on blood analyses that are invasive and episodic, often requiring physical visits to medical facilities, labour-intensive sample processing and storage, and delicate instrumentation (for example, gas chromatography–mass spectrometry (GC–MS))[14]. As the current COVID-19 pandemic remains uncontrolled around the world, there is a pressing need for developing wearable and telemedicine sensors to monitor an individual's health state and to enable timely intervention under home- and community-based settings[15–23]; it is also increasingly important to monitor a person's long-term cardiometabolic and nutritional health status after recovery from severe COVID-19 infection using wearables to capture early signs of potential endocrinological complications such as T2DM[12].

Sweat is an important body fluid containing a wealth of chemicals reflective of nutritional and metabolic conditions[24–27]. The progression from blood analyses to wearable sweat analyses could provide great potential for non-invasive, continuous monitoring of physiological biomarkers critical to human health[28–38]. However, currently reported wearable electrochemical sensors focus primarily on a limited number of analytes including electrolytes, glucose and lactate, owing to the lack of a suitable continuous monitoring strategy beyond ion-selective and enzymatic electrodes or direct oxidation of electroactive molecules[25–27,34–40]. Thus, most clinically relevant nutrients and metabolites in sweat are rarely explored and undetectable by existing wearable sensing technologies. Moreover, current wearable biosensors usually require vigorous exercise to access sweat; although a few recent reports use pilocarpine gel-based iontophoresis for sedentary sweat sampling[22,30,36], this approach suffers from short sweat periods and low sensing accuracy due to the mixing of sweat and gel fluid and the lack of dynamic sweat sampling.

In this Article, we present a universal wearable biosensing strategy based on a judicious combination of the mass-producible laser-engraved graphene (LEG), electrochemically synthesized redox-active nanoreporters (RARs) and molecularly imprinted polymer (MIP)-based 'artificial antibodies', as well as unique in situ regeneration and calibration technologies (Fig. 1b). Unlike bio-affinity sensors based on antibodies or classic MIPs, which are generally for one-time use and require multiple washing steps

[1]Andrew and Peggy Cherng Department of Medical Engineering, Division of Engineering and Applied Science, California Institute of Technology, Pasadena, CA, USA. [2]Department of Applied Physics and Materials Science, Division of Engineering and Applied Science, California Institute of Technology, Pasadena, CA, USA. [3]Department of Electrical Engineering, Division of Engineering and Applied Science, California Institute of Technology, Pasadena, CA, USA. [4]Department of Hematologic Malignancy Translational Sciences, Beckman Research Institute at City of Hope, Duarte, CA, USA. [5]Division of Cardiology, David Geffen School of Medicine, University of California, Los Angeles, CA, USA. [6]Division of Clinical Nutrition, David Geffen School of Medicine, University of California, Los Angeles, CA, USA. [7]These authors contributed equally: Minqiang Wang, Yiran Yang, Jihong Min. ✉e-mail: weigao@caltech.edu

Fig. 1 | Schematics and images of the wearable biosensor 'NutriTrek'. a, Circulating nutrients such as AAs are associated with various physiological and metabolic conditions. **b**, Schematic of the wearable 'NutriTrek' that enables metabolic monitoring through a synergistic fusion of LEG, RARs and artificial antibodies. **c**,**d**, Schematic (**c**) and layer assembly (**d**) of the microfluidic 'NutriTrek' patch for sweat induction, sampling and biosensing. T, temperature. **e**,**f**, Images of a flexible sensor patch (**e**) and a skin-interfaced wearable system (**f**). Scale bars, 5 mm (**e**) and 2 cm (**f**). **g**, Block diagram of electronic system of 'NutriTrek'. The modules outlined in red dashes are included in the smartwatch version. CPU, central processing unit; POT, potentiometry; In-Amp, instrumentation amplifier; MCU, microcontroller; TIA, trans-impedance amplifier; IP, iontophoresis; CE, counter-electrode; RE, reference electrode; WE, working electrode. **h**, Custom mobile application for real-time metabolic and nutritional tracking. **i**, 'NutriTrek' smartwatch with a disposable sensor patch and an electrophoretic display. Scale bars, 1 cm (top) and 5 cm (bottom).

to transduce the bio-affinity interactions in standard ionic solutions[41,42], this approach enables the demonstration of sensitive, selective and continuous monitoring of a wide range of trace-level biomarkers in biofluids including all nine essential AAs as well as vitamins, metabolites and lipids commonly found in human sweat (Supplementary Table 1). Seamless integration of this unique

approach with in situ signal processing and wireless communication leads to a powerful wearable sweat sensing technology 'NutriTrek' that is able to perform personalized and non-invasive metabolic and nutritional monitoring towards timely intervention (Fig. 1b). The incorporation of the carbachol iontophoresis-based sweat induction and efficient microfluidic-based surrounding sweat sampling enables prolonged autonomous and continuous molecular analysis with high temporal resolution and accuracy across activities, during physical exercise and at rest. Using five essential or conditionally essential AAs (that is, Trp, Try and three BCAAs (Leu, Ile and Val)) as exemplar nutrients, we corroborated the system in several human trials by enroling both healthy subjects and patients towards personalized monitoring of central fatigue, standard dietary intakes, nutrition status, metabolic syndrome risks and COVID-19 severity.

Results

Design and overview of the autonomous wearable biosensor technology. The flexible and disposable sensor patch consists of two carbachol-loaded iontophoresis electrodes, a multi-inlet microfluidic module, a multiplexed MIP nutrient sensor array, a temperature sensor and an electrolyte sensor (Fig. 1c–f and Supplementary Fig. 1). All flexible electrode and sensor designs are based on the LEG, which has large surface area, has excellent electrochemical properties and can be produced at a large scale directly on a polyimide (PI) substrate via CO_2 laser engraving (Supplementary Fig. 2). The sensor patch can be easily attached to skin with conformal contact and interfaces with a miniaturized electronic module for on-demand iontophoresis control, in situ signal processing and wireless communication with the user interfaces through Bluetooth (Fig. 1g and Supplementary Figs. 3 and 4). A custom mobile app 'NutriTrek' was developed to process, display and store the dynamic metabolic information monitored by the wearable sensors (Fig. 1h and Supplementary Video 1). The wearable system was also integrated into a smartwatch with an electronic paper display (Fig. 1i and Supplementary Fig. 5).

Biosensor design and evaluation for universal metabolic and nutritional analysis. Universal detection of AAs and other metabolites/nutrients with high sensitivity and selectivity was achieved through careful design of the selective binding MIP layer on the LEG. MIPs are chemically synthesized receptors formed by polymerizing functional monomer(s) with template molecules. Although MIP technology has been proposed for sensing, separation and diagnosis[42,43], it has not yet been demonstrated for continuous wearable sensing as classic MIP sensors require washing steps for sensor regeneration and the detection is generally performed in standard buffer or redox solutions. In our case, the functional monomer (for example, pyrrole) and crosslinker (for example, APBA) initially form a complex with the target molecule; following polymerization, their functional groups are embedded in the polymeric structure on the LEG; subsequent extraction of the target molecules reveals binding sites on the LEG-MIP electrode that are complementary in size, shape, and charge to the target analyte (Supplementary Fig. 6). Two detection strategies—direct and indirect—are designed on the basis of the electrochemical properties of the target molecules (Fig. 2). Optimizations and characterizations of the LEG–MIP sensors are detailed in Supplementary Note 1 and Supplementary Figs. 7–13.

For electroactive molecules in sweat, the oxidation of bound target molecules in the MIP template can be directly measured by differential pulse voltammetry (DPV) in which the peak current height correlates with analyte concentration (Fig. 2a). Considering that multiple electroactive molecules can be oxidized at similar potentials, this LEG–MIP approach addresses both sensitivity and selectivity issues. For example, Tyr and Trp, two AAs with close redox potentials (~0.7 V), could be detected selectively with this strategy (Fig. 2b,c and Supplementary Fig. 14). Linear relationships between peak height current densities and target concentrations with sensitivities of 0.63 $\mu A\,\mu M^{-1}\,cm^{-2}$ and 0.71 $\mu A\,\mu M^{-1}\,cm^{-2}$ respectively for the LEG–MIP Tyr and Trp sensors were observed (Supplementary Fig. 15). It is worth noting that choices of monomer/crosslinker/template ratios and incubation periods have substantial influences on sensor response while sample volume does not (Supplementary Fig. 10). The Tyr and Trp sensors can be readily and repeatably regenerated in situ without any washing step with a high-voltage amperometry current–time (*IT*) that oxidizes the bound targets at their redox potentials (Fig. 2d).

As the majority of metabolites and nutrients (for example, BCAAs) are non-electroactive and cannot easily be oxidized under operational conditions, we herein utilize an indirect detection approach involving an RAR layer sandwiched between the LEG and MIP layers to enable rapid quantitation (Fig. 2e). The selective adsorption of the target molecules onto the imprinted polymeric layer decreases the exposure of the RAR to the sample matrix. Controlled-potential voltammetric techniques such as DPV or linear sweeping voltammetry (LSV) can be applied to measure the RAR's oxidation or reduction peak, where the decrease in peak height current density corresponds to an increase in analyte levels. For example, using Prussian Blue nanoparticles (PBNPs) as the RAR (Supplementary Fig. 11), we developed an MIP–LEG Leu sensor with a log-linear relationship between the peak height decrease and Leu concentration and a sensitivity of 702 $nA\,mm^{-2}$ per decade of concentration (Fig. 2f). We established this approach to quantify the physiologically relevant range of all nine essential AAs (that is, Leu, Ile, Val, Trp, Phe, histidine (His), lysine (Lys), methionine (Met) and threonine (Thr)) (Fig. 2g and Supplementary Fig. 16) as well as a number of vitamins, metabolites and lipids (vitamins B_6, C, D_3 and E, glucose, uric acid, creatine, creatinine and cholesterol) (Fig. 2h and Supplementary Fig. 17). In addition to these nutrients and metabolites, this approach can be easily reconfigured to enable the monitoring of a broad spectrum of biomarkers ranging from hormones (for example, cortisol) to drugs (for example, immunosuppressive drug mycophenolic acid) (Supplementary Fig. 18 and Supplementary Tables 2 and 3). Most of these targets are undetectable continuously by any existing wearable technology. Considering that a total level of multiple nutrients (for example, total BCAAs) is often an important health indicator, a multi-template MIP approach can be used to enable accurate and sensitive detection of the total concentration of multiple targets with a single sensor (Fig. 2i,j). These indirect LEG–RAR–MIP sensors can be regenerated in situ by applying constant potential to the working electrode, which repels the bound target molecules from the MIP layer, achieving prolonged re-usability (Fig. 2k).

The LEG–MIP sensors show stable responses during repeatable use: the PBNP-based RAR showed stable redox signals throughout 60 repetitive cyclic voltammetry (CV) scans (Fig. 2l and Supplementary Fig. 11); minimal output changes were observed throughout a 42-day storage period (Supplementary Fig. 19a,b); the sensors also showed no substantial relative signal shift when used continuously over 5 days (Supplementary Fig. 19c). Compared with traditional MIP preparation processes, the electrodeposited MIP layer on the mass-producible LEG leads to high reproducibility in selectivity, sensitivity and device-to-device consistency (Supplementary Figs. 20 and 21). The choice of LEG as the MIP deposition substrate also showed advantages in sensor sensitivity compared with classic electrodes such as glassy carbon electrode, printed carbon electrode and Au electrode (Supplementary Fig. 22). Other RARs such as anthraquinone-2-carboxylic acid (AQCA) can also be used for indirect AA sensing with stable performance (negatively scanned DPV was used here to monitor AQCA reduction) (Fig. 2m and Supplementary Fig. 23). As illustrated in Fig. 2n, the LEG–AQCA–MIP sensors could be directly regenerated in a raw

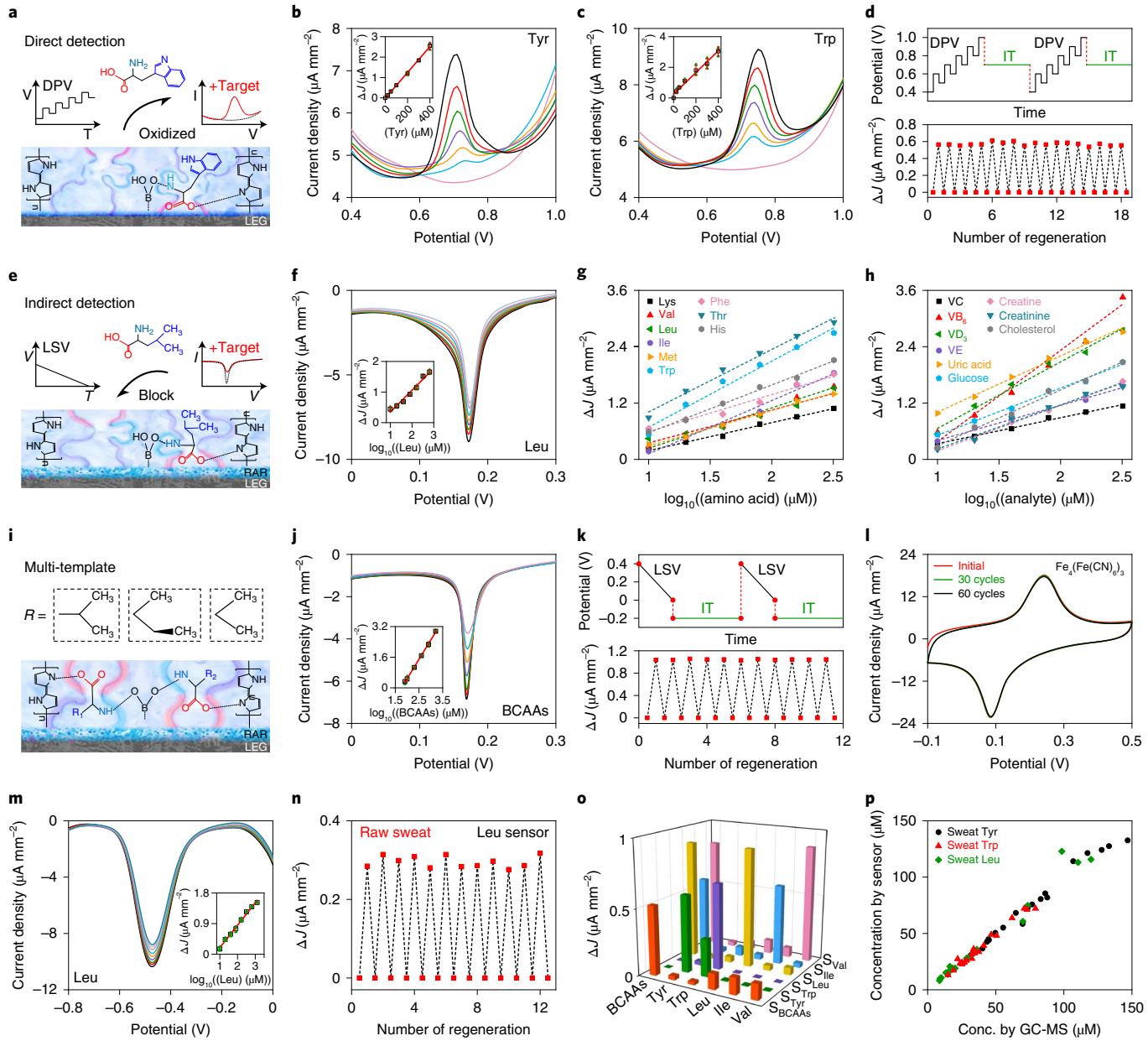

Fig. 2 | Schematics and characterizations of the LEG-MIP sensors. a, Direct detection of electroactive molecules using LEG-MIP sensors. **b**,**c**, DPV voltammograms of the LEG-MIP sensors for direct Tyr (**b**) and Trp (**c**) detection. Insets, calibration plots with a linear fit. Δ*J*, peak height current density. **d**, In situ continuous sensing and regeneration of an LEG-MIP Trp sensor in 50 μM Trp. **e**, Indirect molecular detection using LEG-RAR-MIP sensors. **f**, LSV voltammograms of indirect Leu detection with LEG-PBNP-MIP sensors. Inset, calibration plot with a linear fit. **g**,**h**, Indirect detection of all essential AAs (**g**) and multiple vitamins, lipids and metabolites (**h**) using LEG-PBNP-MIP sensors. Dashed lines represent linear-fit trendlines. VC, vitamin C; VB_6, vitamin B_6; VD_3, vitamin D_3; VE, vitamin E. **i**, Schematic of multi-MIP AA sensors. **j**, LSV voltammograms of an LEG multi-MIP sensor for BCAA quantification. Inset, calibration plot with a linear fit. **k**, In situ continuous sensing and regeneration of an LEG-PBNP-MIP Leu sensor in 50 μM Leu. **l**, Repetitive CV scans of an LEG-PBNP electrode in 0.1 M KCl. **m**, DPV voltammograms of indirect Leu detection with LEG-AQCA-MIP sensors. Inset, the calibration plot. **n**, In situ regeneration of an LEG-AQCA-MIP Leu sensor in a raw sweat sample. **o**, Selectivity of the Trp, Tyr, Leu, Ile, Val and BCAA sensors against other AAs. **p**, Validation of Tyr, Trp and Leu sensors for analysing raw exercise sweat samples ($n = 20$) against GC-MS. All error bars represent the standard deviation (s.d.) from three sensors.

human sweat sample, resolving a main bottleneck of wearable biosensing. The MIP–LEG AA sensors have excellent selectivity for other analytes in sweat (including AAs with similar structures) at physiologically relevant concentrations (Fig. 2o, Supplementary Fig. 24 and Supplementary Table 3). The LEG–MIP technology showed a comparable sensitivity with the current gold-standard laboratory-based GC–MS[44] (Supplementary Fig. 25); the sensor measurements in raw human sweat samples have been validated against GC–MS (Fig. 2p and Supplementary Figs. 26 and 27).

Wearable system design for autonomous sweat induction, sampling, analysis and calibration. To enable on-body continuous metabolic and nutritional monitoring, the flexible sensor patch was designed to comprise an iontophoresis module for localized

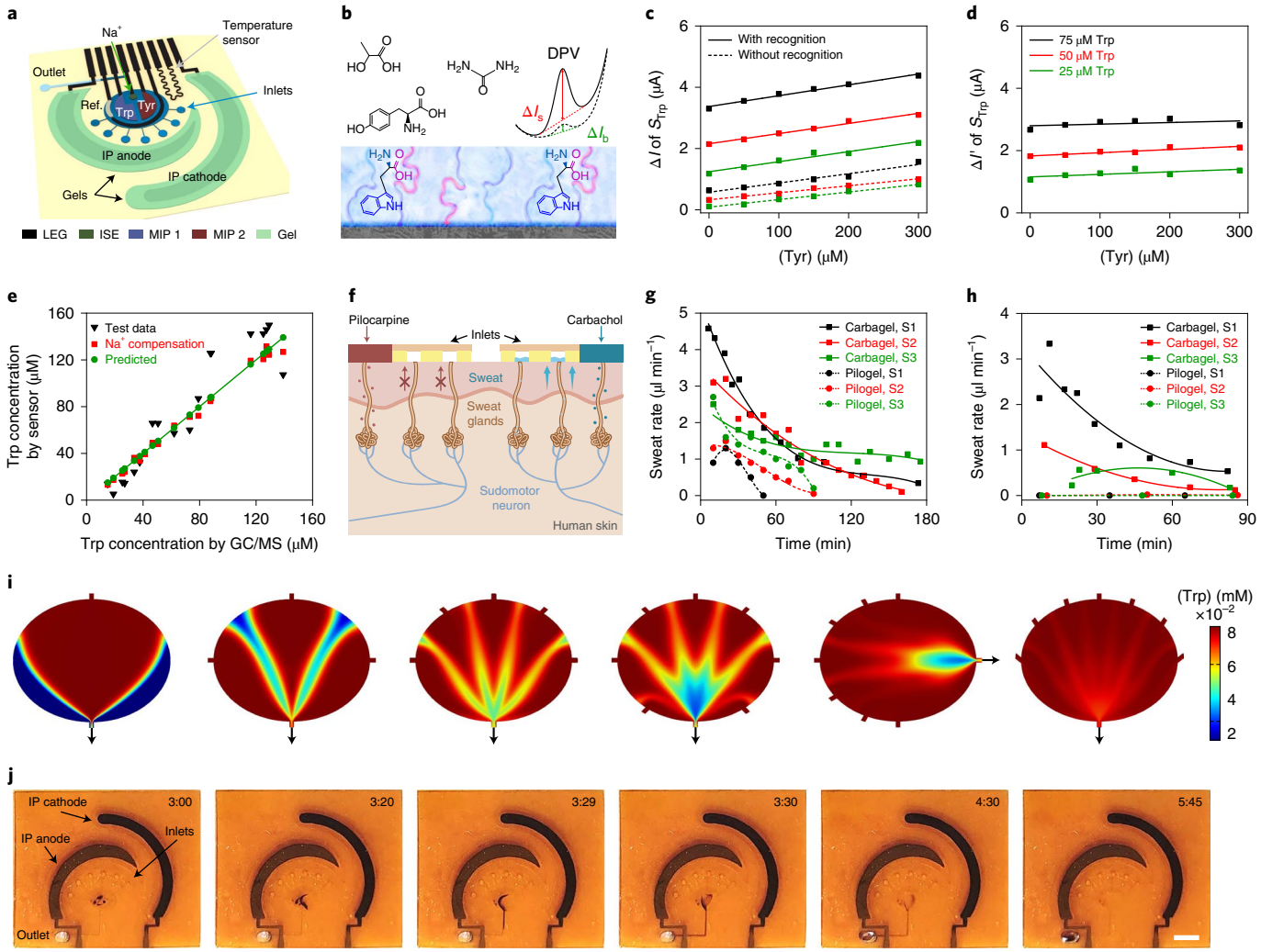

Fig. 3 | Wearable system design for autonomous sweat induction, sampling, analysis and calibration. a, Illustration of a multi-functional wearable sensor patch. ISE, ion-selective electrode. **b**–**d**, The two-scan sensor calibration strategy enabling selective Trp sensing in situ in the presence of Tyr. Δ*I*, peak height current; Δ*I*′, peak height difference caused by target recognition. Solid and dashed curves in **c** and **d** represent linear-fit trendlines. **e**, Electrolyte calibration of the AA sensor reading, with a linear fit. **f**, Schematic of localized sweat sampling based on iontophoretic sweat extraction with muscarinic agents: pilocarpine and carbachol. **g**,**h**, Localized sweat rates measured from the stimulated (**g**) and surrounding (**h**) skin areas after a 5-min iontophoresis with pilocarpine and carbachol. Solid and dashed curves represent quadratic-fit trendlines. S, subject. **i**, Numerically simulated Trp concentration ([Trp]) distributions in the microfluidic reservoir at 120 s after the inlet fluid changed from 20 to 80 μM Trp (flow rate 1.5 μl min^{-1}) (with varied designs in inlet number, angle span, and inlet and outlet orientation). **j**, On-body evaluation of the optimized flexible microfluidic patch for efficient carbachol-based iontophoretic sweat induction and surrounding sampling at rest. Timestamps represent the period (min) after a 5-min iontophoresis session. Black dye was used in the reservoir to facilitate the direct visualization of sweat flow in the microfluidics. Scale bar, 3 mm.

on-demand sweat induction, a multi-inlet microfluidic module for efficient sweat sampling, a multiplex LEG–MIP sweat nutrient sensor array for continuous AA analysis, and LEG-based temperature and electrolyte sensors for real-time AA sensor calibration (Fig. 3a). Unlike classic bio-affinity sensor's detection in buffer or redox solutions, in situ sweat analysis poses more challenges due to complex and interpersonally varied sweat composition and demands technological innovations for accurate on-body sensing. For example, for direct LEG–MIP Trp sensing, a DPV scan in sweat even before target/MIP recognition could lead to an oxidation peak as a small amount of electroactive molecules (for example, Trp and Tyr) can be oxidized on the surface of MIP layer; after recognition and binding of Trp into the MIP cavities, a substantially higher current peak height can be obtained; measuring difference of the two peak heights allows more accurate measurement of bound Trp directly in sweat with high selectivity (Fig. 3b–d). The influence of temperature and ionic strength on the AA sensors can be calibrated in real time on the basis of the readings from an LEG-based strain-resistive temperature sensor and an ion-selective Na^+ sensor (Fig. 3e and Supplementary Fig. 28). Considering that sweat rate during exercise was reported to influence certain biomarker levels, we could use sweat Na^+ level (which showed a linear correlation with sweat rate) to further calibrate the nutrient levels for personalized analysis. This unique transduction strategy involving both the two-step DPV scans and the temperature/electrolyte calibrations allows us to obtain accurate reading continuously in sweat during on-body use (Supplementary Fig. 29).

To make this wearable technology broadly applicable, particularly for sedentary individuals, we utilize here a custom-designed iontophoresis module consisting of the LEG anode and cathode coupled with hydrogels containing muscarinic agent carbachol (carbagel) for sustainable sweat extraction. Carbachol was selected

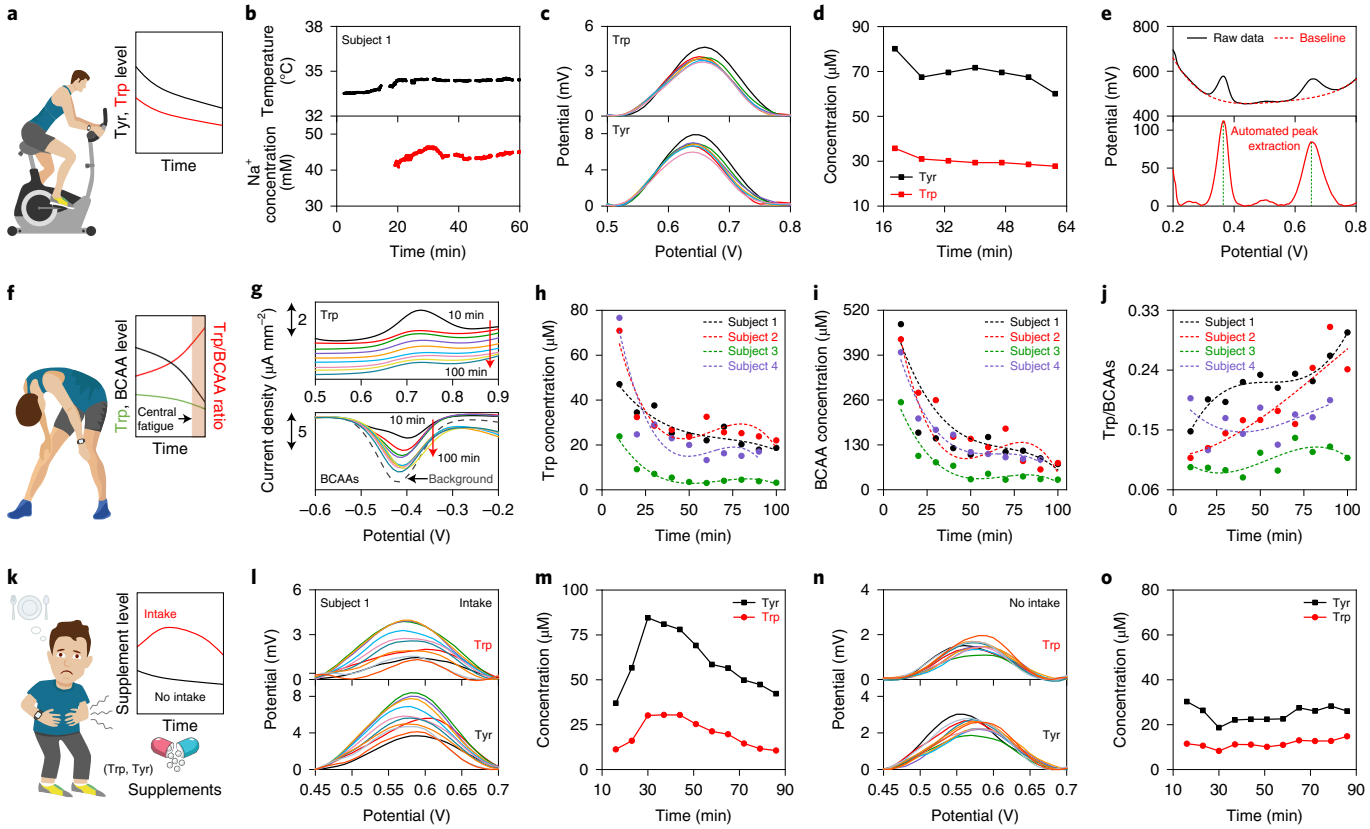

Fig. 4 | Wearable system evaluation across activities towards prolonged physiological and nutritional monitoring. a–d, Continuous on-body Trp and Tyr analysis using a wearable sensor array with real-time sensor calibrations during cycling exercise. **e**, Custom voltammogram analysis with an automatic peak extraction strategy based on a polynomial fitting and cut-off procedure. **f–j**, Dynamic sweat Trp and BCAA analysis during physical exercise towards central fatigue monitoring. Dashed lines in **h–j** represent quadratic fit trendlines. **k–o**, Dynamic analysis of sweat AA levels with and without Trp and Tyr supplement intake at rest towards personalized nutritional monitoring.

from various muscarinic agents as it allows the most efficient, repeatable and long-lasting sweat secretion from the surrounding sweat gland owing to its additional nicotinic effects[45] (Fig. 3f–h, Supplementary Fig. 30 and Supplementary Note 2). In contrast, the classic sweat-inducing agent—pilocarpine—used by the standard sweat test and previously reported wearable systems[22,30,36] offers only a short period of sweat and very limited sweat rate from the neighbouring sweat glands (Fig. 3f–h). Furthermore, sampling the mixture of the leaked sweat underneath the pilocarpine gel and the gel fluid could result in substantial wearable sensor errors and fail to provide real-time information owing to the absence of efficient sweat refreshing. A very small current (50–100 μA) is used for our iontophoresis module, compared with commonly used 1–1.5 mA (refs. [22,30,36]), greatly reducing the risk of skin irritation. To maximize the efficiency of low-volume sweat sampling and improve the temporal resolution of wearable sensing, a compact and flexible microfluidic module was carefully designed to isolate sweat sampling areas from iontophoresis gels. Numerical simulations were performed to optimize the geometric design of the microfluidic module, including inlet number, angle span, orientation and flow direction with respect to the reservoir geometry (Fig. 3i, Supplementary Note 3, Supplementary Figs. 31 and 32, Supplementary Video 2 and Supplementary Table 4). With the optimized design for sweat induction and sampling, sweat can be conveniently induced locally and readily sampled with the multi-inlet microfluidics over a prolonged period (Fig. 3g,j, Supplementary Fig. 33 and Supplementary Video 3). At the physiological sweat rates ranging from 0.15 μl min^{-1} to 3 μl min^{-1}, our wearable sensor patch could provide reliable and accurate analysis of the dynamic changes of the AA levels (Supplementary Figs. 34 and 35).

Evaluation of the wearable system for dynamic physiological and nutritional monitoring. Evaluation of the wearable system was conducted first via sensing of sweat Trp and Tyr in human subjects during a constant-load cycling exercise trial (Fig. 4a–d and Supplementary Fig. 36). The DPV data from the sensors were wirelessly transmitted along with temperature and Na^+ sensor readings to the mobile app that automatically extracted the oxidation peaks using a custom-developed iterative baseline correction algorithm (Fig. 4e and Supplementary Fig. 37) and performed calibration for the accurate quantification of sweat Tyr and Trp. Considering that AAs (for example, Try and BCAAs) play a crucial role in central fatigue during physical exercise[46], a flexible Trp and BCAA sensor array was used to monitor the AA dynamics during vigorous exercise (Fig. 4f–j and Supplementary Fig. 38). Both Trp and BCAA levels decreased during the exercise owing to the serotonin synthesis and BCAA ingestion, respectively. The increased sweat Trp-to-BCAA ratio was observed, which could potentially serve as an indicator of central fatigue, in agreement with a previous report on its plasma counterpart[46].

The wearable iontophoresis-integrated patch enables daily continuous AA monitoring at rest beyond the physical exercise. As illustrated in Fig. 4k–o and Supplementary Figs. 39–42, rising Trp and Tyr levels in sweat were observed from all four subjects after Trp and Tyr supplement intake while the readings from the sensors remained stable during the studies without intake. Such

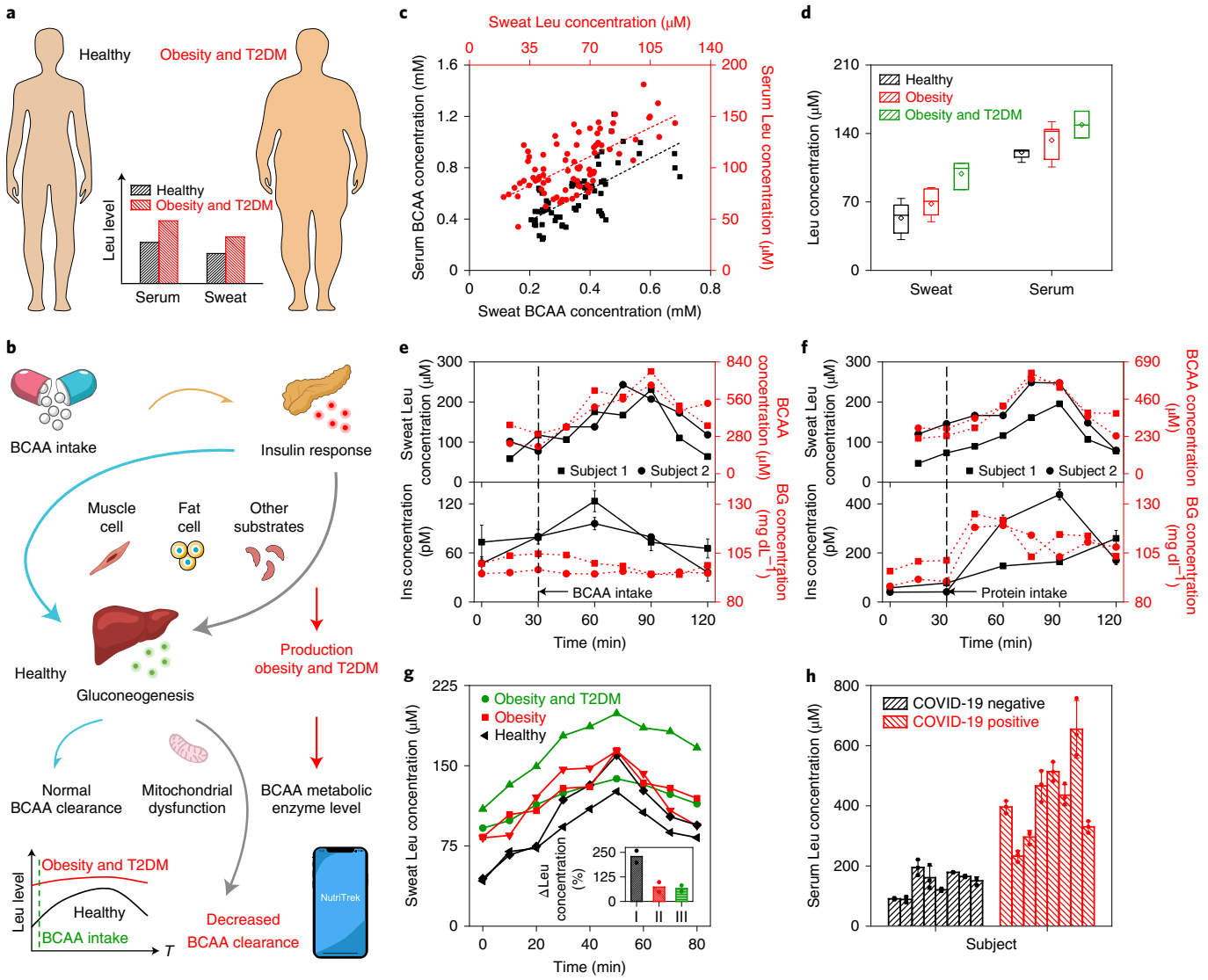

Fig. 5 | Personalized monitoring of metabolic syndrome risk factors using LEG-MIP BCAA sensors. a, Elevated BCAA levels identified in individuals with obesity and/or T2DM. **b**, The close associations between BCAA metabolism and insulin response in healthy and obesity/T2DM groups. **c**, Correlation of serum and sweat total BCAA and Leu levels obtained with the LEG-MIP sensors ($n=65$). Dashed lines represent linear-fit trendlines. **d**, Box-and-whisker plot of measured Leu levels in iontophoresis-extracted sweat and serum in three groups of participants: normal weight (group I, $n=10$), overweight or obesity (group II, $n=7$) and obesity with T2DM (group III, $n=3$), The bottom whisker represents the minimum, the top whisker represents the maximum and the square in the box represents the mean. **e**,**f**, Dynamic changes of sweat Leu and total BCAAs, serum insulin (Ins) and blood glucose (BG) levels from two healthy subjects with 5 g BCAAs (**e**) and standard protein diet (**f**) intakes. **g**, Sweat Leu dynamics collected from groups I–III after 5 g BCAA intake. Inset, ratio of the Leu level at 50 min after BCAA intake and the level before intake. **h**, Evaluation of Leu as a metabolic fingerprint for COVID-19 severity in serum samples from COVID-19-negative subjects ($n=8$) and COVID-19-positive patients ($n=8$). Error bars represent the s.d. from three measurements.

capability opens the door for personalized nutritional monitoring and management through personalized sensor-guided dietary intervention. It should be noted that our pilot study showed that sweat nutrient and electrolyte levels were independent of sweat rate changes during the carbachol-based iontophoresis-induced sweat (Supplementary Fig. 43).

Personalized monitoring of metabolic syndrome risk factors using wireless biosensors. Metabolic syndrome, characterized by abdominal obesity and insulin resistance, is now on the rise as the leading cause of morbidity and mortality, affecting more than a third of all adults in the United States[47]. Elevated circulating BCAAs levels are predictive of insulin-resistant obesity and metabolic syndrome, and are linked to CVDs and T2DM (Fig. 5a and Supplementary Note 4)[3,4], which could lead to potential complications of severe COVID-19 (ref. [12]). Recent studies have shown the potential use of BCAA supplementation as a dietary intervention to ameliorate insulin resistance[48]. Monitoring changes in essential nutrient levels provides highly sensitive early detection of metabolic syndrome risks, enabling effective personalized dietary intervention (Fig. 5b). To explore the use of sweat BCAAs as a non-invasive risk factor of metabolic syndrome, we performed a pilot study to investigate the correlations between serum and sweat BCAAs involving three groups of subjects: normal weight (I, $n=10$), overweight/obesity (II, $n=7$) and obesity with T2DM (III, $n=3$) (Fig. 5c,d). Positive Pearson correlation coefficients of 0.66 ($n=65$) and 0.69 ($n=65$) were observed between sweat and serum levels (all analysed by the sensors) of Leu and total BCAA, respectively (Fig. 5c). Compared

with healthy participants in group I, substantially elevated sweat and serum Leu levels (analysed by the sensors) were observed in groups II and III (Fig. 5d), consistent with previous reports that higher circulating BCAA levels were identified in individuals with obesity and T2DM[3]. Considering the well-established role of BCAAs on insulin production and inhibition of glycogenolysis, we also investigated the post-prandial response of sweat Leu/BCAAs and blood glucose/insulin after BCAA supplement and dietary intake in healthy subjects (Fig. 5e,f). All biomarkers remained stable during the fasting period; protein diet intake resulted in increases in both blood glucose and insulin, while BCAA intake only led to a rapid insulin increase. In both studies, sweat Leu and BCAAs first increased in the 30–60 min and then decreased. For subjects with different metabolic conditions, Leu levels in iontophoretic sweat after BCAA vary differently: although a substantial increase in sweat Leu levels was observed in all cases, healthy subjects showed a drastic percentage fluctuation and individuals with obesity/T2DM showed blunted fluctuation that may indicate the different metabolic stage of BCAA in those individuals (Fig. 5g).

Considering that circulating elevated Leu has been reported as a key metabolic fingerprint for COVID-19 severity, we also evaluated our biosensors for analysing the samples from patients with COVID-19 and healthy individuals; substantially elevated Leu levels were identified in COVID-19-positive samples compared with the negative ones (415.6 ± 133.7 versus $151.5 \pm 36.0\,\mu M$), indicating the great potential of our biosensors for at-home COVID-19 monitoring and management (Fig. 5h).

Discussion

Circulating metabolic biomarkers, such as AAs and vitamins, have been associated with various health conditions, including diabetes and CVDs. Metabolic profiling using wearable sensors has become increasingly crucial in precision nutrition and precision medicine, especially in the era of the COVID-19 pandemic, as it provides not only insights into COVID-19 severity but also guidance to stay metabolically healthy to minimize the risk of potential COVID-19 infection. As the pandemic remains rampant throughout the world and regular medical services are at risk of shortage, there is an urgent need to develop and apply wearable sensors that can monitor health conditions via metabolic profiling to achieve at-home diagnosis and timely intervention via telemedicine. However, current wearable electrochemical sensors are limited to a narrow range of detection targets owing to lack of continuous sensing strategies beyond ion-selective and enzymatic electrodes. Though various bio-affinity-based sensors have been developed to detect a broader spectrum of targets using antibodies or MIPs, they generally require multiple washing steps or provide only one-time use; these limitations have hampered their useability in wearable devices. Moreover, the majority of wearable biosensors rely on vigorous exercise to access sweat and are not suitable for daily continuous use.

By integrating mass-producible LEG, electrochemically synthesized RARs and 'artificial antibodies', we have demonstrated a powerful universal wearable biosensing strategy that can achieve selective detection of a broad range of biomarkers (including all essential AAs, vitamins, metabolites, lipids, hormones and drugs) and reliable in situ regeneration. Furthermore, to enable continuous and on-demand metabolic and nutritional monitoring across the activities, we have integrated the LEG–MIP sensor array and iontophoresis-based sweat induction into a wireless wearable technology, with optimized multi-inlet microfluidic sudomotor axon reflex sweat sampling, in situ signal processing, calibration and wireless communication. Using this telemedicine technology, we have demonstrated the wearable and continuous monitoring of post-prandial AA responses to identify risks for metabolic syndrome. The high correlation between sweat and serum BCAAs suggests that this technology holds great promise for use in metabolic syndrome risk monitoring. The substantial difference in Leu between COVID-19-positive and COVID-19-negative blood samples indicates the potential of using this technology for at-home COVID-19 management. We envision that this wearable technology could play a crucial role in the realization of precision nutrition through continuous monitoring of circulating biomarkers and enabling personalized nutritional intervention. This technology could also be reconfigured to continuously monitor a variety of other biomarkers towards a wide range of personalized preventive, diagnostic and therapeutic applications.

Methods

Materials and reagents. Uric acid, L-tyrosine, silver nitrate, iron(III) chloride, dopamine hydrochloride, choline chloride, creatinine, pantothenic acid calcium salt, citrulline, pyridoxine and lactic acid were purchased from Alfa Aesar. Sodium thiosulfate pentahydrate, sodium bisulfite, tryptophan, leucine, alanine, isoleucine, methionine, valine, lysine, thiamine hydrochloride, serine, sulfuric acid, hydrochloric acid, AQCA, 3-aminophenylboronic acid (APBA), aniline, *o*-phenylenediamine, methylene blue, thionine, 2-(*N*-morpholino)ethanesulfonic acid hydrate (MES), ethanolamine, *N*-(3-dimethyl-aminopropyl)-*N′*-ethylcarbodiimide (EDC), *N*-hydroxysulfosuccinimide sodium salt (sulfo-NHS), bovine serum albumin (BSA), tris(hydroxymethyl)aminomethane hydrochloride (Tris–HCl), streptavidin–peroxidase conjugate (Roche) and hydroquinone were purchased from Sigma-Aldrich. Carboxylic-acid-modified magnetic beads (MBs; Dynabeads, M-270) were obtained from Invitrogen. Potassium ferricyanide and potassium ferrocyanide were purchased from Acros Organics. Acetic acid, methanol, sodium acetate, sodium chloride, sodium dihydrogen phosphate, potassium chloride, potassium hydrogen phosphate, urea, L-ascorbic acid and dextrose (D-glucose) anhydrous, glycine, arginine, inositol, ornithine, aspartic acid, threonine, histidine, riboflavin, creatine, phenylalanine, nicotinic acid, folic acid, glutamic acid and hydrogen peroxide (30% (w/v)) were purchased from Thermo Fisher Scientific. Insulin capture antibody and biotinylated detector antibody were purchased from R&D systems (Human/Canine/Porcine Insulin DuoSet ELISA). Screen printed carbon electrodes and magnetic holder were purchased from Metrohm DropSens. Medical adhesives were purchased from 3 M and Adhesives Research. PI films (75 µm thick) were purchased from DuPont. PET films (12 µm thick) were purchased from McMaster-Carr.

Fabrication and preparation of the LEG sensors. The LEG electrodes were fabricated on a PI film with a thickness of 75 µm (DuPont) with a 50 W CO_2 laser cutter (Universal Laser System). When engraving the PI with a CO_2 laser cutter, the absorbed laser energy is converted to local heat and thus leads to a high localized temperature (>2,500 °C), chemical bonds in the PI network are broken and thermal re-organization of the carbon atoms occurs, resulting in sheets of graphene structures. The optimized parameters for the graphene electrodes and electronic connections were power 8%, speed 15%, and points per inch (PPI) 1,000 in raster mode with three-time scan. For the active sensing area of the temperature sensor, the optimized parameters were power 3%, speed 18%, and PPI 1,000 in vector mode with one-time scan. To prepare the reference electrode, Ag was first modified on the corresponding graphene electrode by multi-current electrodeposition with electrochemical workstation (CHI 832D) at −0.01 mA for 150 s, −0.02 mA for 50 s, −0.05 mA for 50 s, −0.08 mA for 50 s and −0.1 mA for 350 s using a plating solution containing 0.25 M silver nitrate, 0.75 M sodium thiosulfate and 0.5 M sodium bisulfite. To obtain the Ag/AgCl electrode, 0.1 M $FeCl_3$ solution was further dropped on the Ag surface for 30 s, and then 3 µl polyvinyl butyral (PVB) reference cocktail prepared by dissolving 79.1 mg of PVB and 50 mg of NaCl in 1 ml of methanol was dropped on the Ag/AgCl electrode and dried overnight. The Na^+-selective electrode was prepared as follows: 0.6 µl of Na^+-selective membrane cocktail prepared by dissolving 1 mg of Na ionophore X, 0.55 mg sodium tetrakis[3,5-bis(trifluoromethyl)phenyl]borate, 33 mg polyvinyl chloride and 65.45 mg bis(2-ethylhexyl) sebacate into 660 µl of tetrahydrofuran was drop-casted onto the graphene electrode and dried overnight. To obtain the desired stable Na^+-sensing performance for long-term continuous measurements, the obtained Na^+ sensor was conditioned overnight in 100 mM NaCl.

The fabrication process of the LEG–MIP sensor array is illustrated in Supplementary Fig. 6. All the MIP layers are synthesized by electro-polymerization. The polymerization solution was prepared by dissolving 5 mM template (for example, target AA), 12.5 mM APBA and 37.5 mM pyrrole into 0.01 M phosphate-buffered saline (PBS) (pH 6.5). For multi-MIP BCAA sensor, 5 mM of each target (that is, Leu, Ile and Val) was used. Before MIP deposition, the LEG was activated in 0.5 M H_2SO_4 with CV scans for 60 segments (−1.2 to 1 V with a scan rate of 500 mV s^{-1}). For the direct-detection LEG–MIP sensors, the target imprinted polymer was electrochemically synthesized on the LEG electrode with CV deposition (0–1 V for ten cycles, 50 mV s^{-1}) using the prepared polymerization solution. The target molecules were extracted by soaking the electrode into an acetic acid/methanol mixture (7:3 v/v) for 1 h. Subsequently, the resulting electrode was immersed into 0.01 M PBS (pH 6.5) for repetitive

CV scans (0.4–1 V with a scan rate of 50 mV s^{-1}) until a stable response was obtained. For LEG-non-imprinted polymer, the electrode was prepared following the same procedure as LEG–MIP except that no template was added in the polymerization solution.

For the indirect-detection MIP sensors, electrochemically synthesized RARs (for example, PBNPs or AQCA) were first modified on the LEG electrode. The PBNP RAR on the LEG was prepared with CV (20 cycles) (−0.2 to 0.6 V with a scan rate of 50 mV s^{-1}) in an aqueous solution containing 3 mM $FeCl_3$, 3 mM $K_3Fe(CN)_6$, 0.1 M HCl and 0.1 M KCl. A PBNP layer with appropriate redox signal is necessary to produce a good sensitivity for the final MIP sensors; to achieve this stable and suitable redox signal, the LEG electrode was rinsed with distilled water after the initial Prussian blue (PB) deposition, and the PB electrodeposition step was repeated two more times until a stable 70 µA LSV peak in 0.1 M KCl solution was achieved. Subsequently, the LEG–PB was rinsed with distilled water and immersed in a solution containing 0.1 M HCl and 0.1 M KCl for repetitive CV scans (−0.2 to 0.6 V with a scan rate of 50 mV s^{-1}) until a stable response was obtained. To prepare the AQCA RAR on the LEG, the LEG electrode was first incubated in 50 µl PBS (pH 6.5) with 5 mM AQCA at 4 °C overnight. Subsequently, the LEG–AQCA was rinsed with distilled water and immersed into a phosphate buffer solution for repetitive CV scans (−0.8 to 0 V with a scan rate of 50 mV s^{-1}) until a stable response was obtained. For the indirect-detection LEG–PB–MIP sensors, an additional PB activation process was conducted right after the template extraction (IT scan at 1 V in 0.5 M HCl for 600 s), followed by an LEG–PB–MIP sensor stabilization process in 0.1 M KCl (CV scans at −0.2 to 0.6 V with a scan rate of 50 mV s^{-1}). It should be noted that, for the LEG–AQCA–MIP sensor, only three CV cycles of polymerization were used to prepare the MIP layer, and the sensor was stabilized in 0.01 M PBS (pH 6.5) (CV scans at −0.8 to 0 V with a scan rate of 50 mV s^{-1}).

The morphology of materials was characterized by scanning electron microscopy (Nova Nano SEM 450) and transmission electron microscopy (Talos S-FEG FEI, USA). The Raman spectrum of the electrodes with different modification was recorded using a 532.8 nm laser with an inVia Reflex (Renishaw). Fourier-transform infrared spectra were measured using infrared spectrometry (Nicolet 6700).

Characterization of the LEG sensor performance. A set of electrochemical sensors were characterized in solutions of target analytes. All the in vitro sensor characterizations were performed through CHI 832D. The response of the Na^+ sensor was characterized with open circuit potential measurements in the solutions containing varied Na^+ levels. DPV analysis was performed for all the direct-detection LEG–MIP sensor characterizations in 0.01 M PBS (pH 6.5) or in raw sweat. The DPV conditions were as follows: range, 0.4–1 V; incremental potential, 0.01 V; pulse amplitude, 0.05 V; pulse width, 0.05 s; pulse period, 0.5 s; and sensitivity, 1×10^{-5} A V^{-1}. For in vitro indirect detection of the target molecules based on the LEG–PB–MIP sensors, LSV analysis (0.4–0 V) was performed in 0.1 M KCl. The LSV conditions were as follows: range, 0.4–0 V; scan rate, 0.005 V s^{-1}; sample interval, 0.001 V; quiet time, 2 s; and sensitivity, 1×10^{-4} A V^{-1}. For in vitro indirect detection of the target molecules based on the LEG–AQCA–MIP sensors, negative DPV analysis (0 to −0.8 V) was performed in 0.01 M PBS. The negative DPV conditions were as follows: 0 to −0.8 V; incremental potential, 0.01 V; pulse amplitude, 0.05 V; pulse width, 0.05 s; pulse period, 0.5 s; and sensitivity, 1×10^{-5} A V^{-1}. For in situ sweat analyte measurement, background and signal curves were recorded before and after incubation; the signal current was obtained as the difference of the peak amplitudes between the post-incubation signal and the background current curves (Fig. 3b–d and Supplementary Fig. 29). The temperature sensor characterization was carried out on a ceramic hot plate (Thermo Fisher Scientific) (Supplementary Fig. 28). The sensor response was recorded using a parameter analyser (Keithley 4200A-SCS) and compared with the readings from an infra-red thermometer (LASERGRIP 800; Etekcity).

To evaluate the performance of the various electrode substrates for MIP-based AA sensing, LEG, printed carbon electrode, Au electrode and glassy carbon electrode were chosen. The glassy carbon electrodes were purchased from CH Instruments. The printed carbon electrodes were printed on the PI substrate using a Dimatix Materials Printer DMP-2850 (Fujifilm, Minato, Japan) with a commercial carbon ink from NovaCentrix. The Au electrodes were fabricated via E-beam evaporation: 20 nm of Cr and 100 nm of Au were deposited onto an O_2-plasma pre-treated PET substrate. MIP films were prepared with CV deposition (0–1 V for ten cycles, 50 mV s^{-1}).

Fabrication and characterization of microfluidic channels. The microfluidic module was fabricated using a 50 W CO_2 laser cutter (Universal Laser System) (Supplementary Fig. 1). Briefly, layers of double-sided and single-sided medical adhesives (3M) were patterned with channels, inlets, the iontophoresis gel outlines and reservoirs. For all microfluidic layers, the iontophoresis gel outlines were patterned to enable the current flow from the top PI electrode layer. The bottom layer, which is the double-sided adhesive layer in contact with the skin (accumulation layer), was patterned with a sweat accumulation well (3M 468MP, laser parameters: power 60%, speed 90%, PPI 1,000). The second layer (the inlet layer), in contact with the accumulation layer, was patterned with the multiple inlets (12-µm-thick PET, laser parameters: power 20%, speed 100%, PPI 1,000). The third layer (channel layer), in contact with the inlets layer, was patterned with microfluidic channels (Adhesives Research 93049, laser parameters: power 45%, speed 100%, PPI 1,000). The fourth layer (reservoir layer), sandwiched between the channel layer and the electrode PI layer, was patterned with the reservoir and the outlet (3M 468MP, laser parameters: power 60%, speed 90%, PPI 1,000). The reservoir is an ellipse with a 5.442 mm major axis and a 4.253 mm minor axis to fully enclose the active sensing area. The thickness of the channel layer is ~0.1 mm (Adhesives Research 93049), and the thickness of the reservoir layer is 0.13 mm (3M 468MP). The reservoir area is 18.17 mm^2, and thus the reservoir volume can be calculated as the area multiplied by the thickness of the reservoir layer (0.13 mm), which totals 2.36 µl.

Fabrication of agonist agent hydrogels. Hydrogels containing muscarinic agent carbachol was prepared as follows. Briefly, for anode gel, agarose (3% w/w) was added into de-ionized water and then heated to 250 °C under constant stirring. After the mixture was fully boiled and became homogeneous without agarose grains, the mixture was cooled down to 165 °C and 1% carbachol was added to the above mixture. Subsequently, the cooled mixture was slowly poured into pre-made cylindrical moulds or into assembled microfluidic patch and solidified for 10 min at 4 °C. The cathode gel was prepared similarly except that NaCl (1% w/w) was used instead of carbachol.

Signal conditioning, processing and wireless transmission for the wearable sensor. The block diagram of the electronic system (Fig. 1g and Supplementary Fig. 4) represents both the wearable electronic patch and the smart watch that can (1) induce sweat via iontophoresis and (2) monitor sweat via electrochemical methods. The sweat induction and the sweat sensing procedures are initiated and controlled by the microcontroller (STM32L432KC, STMicroelectronics) when it receives a user command from the Bluetooth module over universal asynchronous receiver–transmitter (UART) communication.

Sweat induction. Programmable iontophoretic current is generated by a voltage-controlled current source that consists of a unity-gain difference amplifier (AD8276, Analog Devices) and a boost transistor (BC846, ON Semiconductor). The circuit is supplied by the output of a boost converter (LMR64010) that boosts the 3.7 V battery voltage to 36 V. The microcontroller controls the digital-to-analogue converter (DAC) (DAC8552, Texas Instruments) over a serial peripheral interface to set the control voltage of the current source. The current source output is checked by a comparator (TS391, STMicroelectronics), and the microcontroller is interrupted through its general-purpose input/output pin at output failure. The protection circuit consists of a current limiter (MMBF5457, ON Semiconductor) and analogue switches (MAX4715, Maxim Integrated; ADG5401, Analog Devices). The microcontroller's general-purpose input/output is also used to enable or disable the iontophoresis circuit. For the optimized design, a 100-µA current (~2.6 µA mm^{-2}) was applied for on-body iontophoresis sweat induction using the flexible microfluidic patch.

Power analysis. When powered at 3.3 V, the electronic system consumes ~28 mA during an active electrochemical measurement and ~61 mA during iontophoresis. The microcontroller and Bluetooth module each consume ~12 mA; the sensor interface consumes ~4 mA; the boost converter and iontophoresis module consumes ~33 mA; and the display module consumes an additional ~8 mA when refreshing its screen.

Sweat sensing. The sweat sensing circuitry can perform two-channel simultaneous DPV, as well as potentiometric and temperature measurements. A bipotentiostat circuit is constructed by a control amplifier (AD8605) and two transimpedance amplifiers (AD8606). A series voltage reference (ISL60002, Renesas Electronics) and a DAC (DAC8552, Texas Instruments) is used to generate a dynamic potential bias across the reference and working electrodes. An instrumentation amplifier (INA333, Texas Instruments) is used for potentiometric measurements, and a voltage divider is used for the resistive temperature sensor. All analogue voltage signals are acquired by the microcontroller's built-in analogue-to-digital converter (ADC) channels, processed and then transmitted over Bluetooth to a user device.

Custom mobile application design. The custom mobile application was developed with the cross-platform Flutter framework. The mobile application can wirelessly communicate with the wearable devices via Bluetooth to send commands, and to acquire, process and visualize the sweat biomarker levels. The application establishes a secure Bluetooth connection to the wearable sensor. The home page plots the user's historical biomarker levels, and highlights the most recently measured analyte concentrations. When a sweat biomarker measurement is prompted, the user can switch over to the measurement page that plots the sweat sensors' voltammograms in real time. Following the voltammetric measurement, the app extracts the voltammograms' peak currents using a custom baseline correction algorithm, then converts the peak currents to corresponding biomarker concentrations. These measurement data are added to the list of historic analyte levels on the home page.

Refreshing time analysis and simulations. The refreshing time analyses were performed using numerical simulations (COMSOL). Three-dimensional models of different microfluidic designs with same dimensions of the actual device were created in Rhinoceros and imported into COMSOL Multiphysics. The mass transport process was simulated by numerically solving the Stokes equation for an incompressible flow coupled with convection–diffusion equation (Supplementary Note 3).

Human subject recruitment. The validation and evaluation of the sweat sensor were performed using human subjects in compliance with all the ethical regulations under protocols (ID 19-0892 and 21-1079) that were approved by the institutional review board at California Institute of Technology. The participating subjects (aged over 18 years) were recruited from the California Institute of Technology campus and the neighbouring communities through advertisement. All subjects gave written informed consent before study participation. For wearable sensor evaluation, healthy subjects with a body mass index (BMI) of 18.5–24.9 kg m^{-2} with fasting serum glucose <100 mg dl^{-1} were recruited. For the BCAA study, inclusion criteria include: group I, individuals with normal weight who have a BMI of 18.5–24.9 kg m^{-2} with fasting serum glucose <100 mg dl^{-1} (healthy); group II, individuals with overweight/obesity who have a BMI of 25–35 kg m^{-2} and fasting serum glucose <6 mg dl^{-1} (overweight/obesity); group III, individuals with obesity who have a BMI of 25–35 kg m^{-2} and fasting serum glucose ≥126 mg dl^{-1} (obesity and T2DM). COVID-19-positive and COVID-19-negative serum samples were purchased from RayBiotech.

GC–MS analysis for sensor validation. GC–MS analysis of the AAs in sweat and serum samples was performed using EZ:Faast kit from Phenomenex, which enables sample preparation, derivatization and GC–MS analysis of free AAs. A Varian Saturn 2000 was used for the GC–MS runs. One microlitre of prepared sample solution was injected for GC in helium carrier gas at 1.0 ml min^{-1} constant flow with a pulse pressure of 20 pounds per square inch for 0.2 min, with the oven programmed from 110 °C to 320 °C at 32 °C min^{-1}. The mass chromatography was set with source at 240 °C, quad at 180 °C and auxiliary at 310 °C with a scan range of 45–450 *m*/*z* at a sampling rate of 3.5 scans s^{-1}. Selected ion monitoring was used, which records the ion current at selected masses that are characteristic of the certain AA in an expected retention time[49]. For example, after the derivatization of the EZ:Faast kit, Trp has a characteristic mass at 130 with a retention time at around 5.1 min, and peak height is recorded for Trp measurements at ion number 130 and at 5.1 min from the raw data spectrum. The internal standard (IS; norvaline) was added during the sample derivatization process to account for potential evaporation-induced increase in peak detection; the IS norvaline peak height is recorded at its ion number 158 at 1.65 min (Supplementary Fig. 26). The Trp peak height recorded from raw data spectrum was calibrated with respect to the IS in the same run: normalized Trp peak height = Trp peak height/IS peak height. With normalized peak heights of different levels of Trp standards, calibration plots were constructed. For other samples, the normalized peak height of Trp was used to calculate the concentration.

Integrated system validation in human subjects. *System evaluation during exercise.* To validate the wearable sensor system, we conducted constant-load cycling exercise on healthy subjects. The subjects reported to the lab after fasting overnight and were given a standardized protein drink (Fairlife, Core Power Elite). The subjects' foreheads and necks were cleaned with alcohol swabs and gauze before the sensor patches were placed on the body. A stationary exercise bike (Kettler Axos Cycle M-LA) was used for cycling trials. The subjects cycled at 60 rpm for 60 min or until fatigue. During the on-body trial, the data from the sensor patches were wirelessly sent to the user interface via Bluetooth. When the subjects started biking, the sensor system continuously acquired and transmitted temperature and sodium sensor data. Every minute, the electronic system initiated a transient voltage bias between the reference and working electrodes. When the bias triggered a current above an experimentally determined threshold, the system would start a CV cleaning cycle and then the first DPV scan as the initial background without target incubation. The DPV scan was repeated 7 min later as the post-incubation curve. Between the two scans, sodium and temperature sensor data were continuously recorded. Right after the post-incubation DPV, another cycle started with an IT cleaning/regeneration step, followed by an initial background DPV scan. The collected temperature, sodium and DPV data were wirelessly transmitted to a user device via Bluetooth in real time, where the molecular data were extracted, calibrated and converted to concentration levels. Sweat samples were collected periodically from the subjects during the studies using centrifuge tubes. The sweat samples were then frozen at −20 °C for further testing and validation via electrochemical test with the biosensors and GC–MS analysis.

System evaluation with Tyr/Trp supplement intake. The subjects reported to the lab after fasting overnight. The subjects' arms were cleaned with alcohol swabs and gauze before the sensor patches were placed on the body. The subjects were provided Tyr and Trp supplement (1 g each) for the intake study. In contrast, the control study was performed on the subjects without any supplementary intake. Five-minute iontophoresis was applied on the subjects. The sensor data recording process was the same as in exercise-based human trials.

Sensor evaluation with BCAA diet challenge. For the BCAA studies, the subjects were asked to consume 5 g BCAAs (2:1:1 Leu:Ile:Val) or a standardized snack including a protein drink (Fairlife, Core Power Elite) and a CLIF energy bar. An iontophoresis session was implemented with carbachol gels for sweat induction. Over the entire study period, the subject's sweat was sampled periodically and analysed by the sensor patch. Blood glucose level was recorded every 15 min with a commercial Care Touch Blood Glucose Meter. Fresh capillary blood samples were collected using a finger-prick approach during the human studies. After cleaning the fingertip with alcohol wipe and allowing it to air dry, the skin was punctured with a CareTouch lancing device. Samples were collected with centrifuge tubes after wiping off the first drop of blood with gauze. After the 90-min standardized clotting procedure finished, serum was separated by centrifuging at 6,000 rpm for 15 min, and instantly stored at −20 °C for analysis with GC–MS, the LEG–MIP sensors and the custom insulin assay.

Blood insulin analysis. For the BCAA diet challenge study, the collected serum samples were analysed using a custom insulin sandwich immunoassay. The MBs were modified on the basis of a previous publication[50]. Briefly, 3 µl MBs were activated with 50 mg ml^{-1} EDC/sulfo-NHS in MES buffer (25 mM, pH 5) for 35 min followed by capture antibody immobilization (25 µg ml^{-1} in MES buffer) for 15 min. After de-activation with 1 M ethanolamine in phosphate buffer (0.1 M, pH 8), MBs were incubated in 25 µl standards prepared in 1% BSA or serum samples diluted five times in 1% BSA for 15 min. From here, the beads were rinsed with 1% BSA twice after each binding step. Next, the MBs were incubated in 25 µl of biotin-detector antibody (1.0 µg ml^{-1}) in 1% BSA for 30 min followed by 15 min in streptavidin–peroxidase conjugate (2,500×) prepared in 1% BSA. The amperometric detection was carried out by applying a constant potential of −0.2 V to MBs resuspended in 45 µl 1 mM hydroquinone, and 5 µl 5 mM H_2O_2 was pipetted onto the screen-printed carbon electrodes when background current stabilized.

Reporting summary. Further information on research design is available in the Nature Research Reporting Summary linked to this article.

Data availability

The main data supporting the results in this study are available within the paper and its Supplementary Information. Source data for Figs. 4 and 5 and for Supplementary Figs. 36 and 39–41 are provided with this paper. All raw and analysed datasets generated during the study are available from the corresponding author on request. Source data are provided with this paper.

Received: 7 June 2021; Accepted: 19 June 2022;
Published online: 15 August 2022

References

1. Trumbo, P., Schlicker, S., Yates, A. A. & Poos, M. Dietary reference intakes for energy, carbohydrate, fiber, fat, fatty acids, cholesterol, protein and amino acids. *J. Am. Diet. Assoc.* **102**, 1621–1630 (2002).
2. Wu, G. Amino acids: metabolism, functions, and nutrition. *Amino Acids* **37**, 1–17 (2009).
3. Lynch, C. J. & Adams, S. H. Branched-chain amino acids in metabolic signalling and insulin resistance. *Nat. Rev. Endocrinol.* **10**, 723–736 (2014).
4. Wang, T. J. et al. Metabolite profiles and the risk of developing diabetes. *Nat. Med.* **17**, 448–453 (2011).
5. Mayers, J. R. et al. Elevation of circulating branched-chain amino acids is an early event in human pancreatic adenocarcinoma development. *Nat. Med.* **20**, 1193–1198 (2014).
6. Kau, A. L., Ahern, P. P., Griffin, N. W., Goodman, A. L. & Gordon, J. I. Human nutrition, the gut microbiome and the immune system. *Nature* **474**, 327–336 (2011).
7. Fernstrom, J. D. & Wurtman, R. J. Brain serotonin content: physiological dependence on plasma tryptophan levels. *Science* **173**, 149–152 (1971).
8. Fernstrom, J. D. & Fernstrom, M. H. Tyrosine, phenylalanine, and catecholamine synthesis and function in the brain. *J. Nutr.* **137**, 1539S–1547S (2007).
9. Dierckx, T. *et al.* The metabolic fingerprint of COVID-19 severity. Preprint at *medRxiv* (2020) https://doi.org/10.1101/2020.11.09.20228221
10. Grant, W. B. et al. Evidence that vitamin D supplementation could reduce risk of influenza and COVID-19 infections and deaths. *Nutrients* **12**, 988–1006 (2020).
11. Belanger, M. J. et al. COVID-19 and disparities in nutrition and obesity. *N. Engl. J. Med.* **383**, e69 (2020).
12. Stefan, N., Birkenfeld, A. L. & Schulze, M. B. Global pandemics interconnected—obesity, impaired metabolic health and COVID-19. *Nat. Rev. Endocrinol.* **17**, 135–149 (2021).

13. Wishart, D. S. Emerging applications of metabolomics in drug discovery and precision medicine. *Nat. Rev. Drug Discov.* **15**, 473–484 (2016).
14. Dettmer, K., Aronov, P. A. & Hammock, B. D. Mass spectrometry-based metabolomics. *Mass Spectrom. Rev.* **26**, 51–78 (2007).
15. Ray, T. R. et al. Bio-integrated wearable systems: A comprehensive review. *Chem. Rev.* **119**, 5461–5533 (2019).
16. Hollander, J. E. & Carr, B. G. Virtually perfect? Telemedicine for COVID-19. *N. Engl. J. Med.* **382**, 1679–1681 (2020).
17. Niu, S. et al. A wireless body area sensor network based on stretchable passive tags. *Nat. Electron.* **2**, 361–368 (2019).
18. Meng, K. et al. A wireless textile-based sensor system for self-powered personalized health care. *Matter* **2**, 896–907 (2020).
19. Wang, C. et al. Monitoring of the central blood pressure waveform via a conformal ultrasonic device. *Nat. Biomed. Eng.* **2**, 687–695 (2018).
20. Ni, X. et al. Automated, multiparametric monitoring of respiratory biomarkers and vital signs in clinical and home settings for COVID-19 patients. *Proc. Natl Acad. Sci. USA* **118**, e2026610118 (2021).
21. Jeong, H. et al. Differential cardiopulmonary monitoring system for artifact-canceled physiological tracking of athletes, workers, and COVID-19 patients. *Sci. Adv.* **7**, eabg3092 (2021).
22. Sempionatto, J. R. et al. An epidermal patch for the simultaneous monitoring of haemodynamic and metabolic biomarkers. *Nat. Biomed. Eng.* **5**, 737–748 (2021).
23. Xu, C., Yang, Y. & Gao, W. Skin-interfaced sensors in digital medicine: from materials to applications. *Matter* **2**, 1414–1445 (2020).
24. Heikenfeld, J. et al. Accessing analytes in biofluids for peripheral biochemical monitoring. *Nat. Biotechnol.* **37**, 407–419 (2019).
25. Bariya, M., Nyein, H. Y. Y. & Javey, A. Wearable sweat sensors. *Nat. Electron.* **1**, 160–171 (2018).
26. Yang, Y. & Gao, W. Wearable and flexible electronics for continuous molecular monitoring. *Chem. Soc. Rev.* **48**, 1465–1491 (2019).
27. Kim, J., Campbell, A. S., de Ávila, B. E.-F. & Wang, J. Wearable biosensors for healthcare monitoring. *Nat. Biotechnol.* **37**, 389–406 (2019).
28. Gao, W. et al. Fully integrated wearable sensor arrays for multiplexed in situ perspiration analysis. *Nature* **529**, 509–514 (2016).
29. Bandodkar, A. J. et al. Battery-free, skin-interfaced microfluidic/electronic systems for simultaneous electrochemical, colorimetric, and volumetric analysis of sweat. *Sci. Adv.* **5**, eaav3294 (2019).
30. Emaminejad, S. et al. Autonomous sweat extraction and analysis applied to cystic fibrosis and glucose monitoring using a fully integrated wearable platform. *Proc. Natl Acad. Sci. USA* **114**, 4625–4630 (2017).
31. Torrente-Rodríguez, R. M. et al. Investigation of cortisol dynamics in human sweat using a graphene-based wireless mHealth System. *Matter* **2**, 921–937 (2020).
32. Koh, A. et al. A soft, wearable microfluidic device for the capture, storage, and colorimetric sensing of sweat. *Sci. Transl. Med.* **8**, 366ra165 (2016).
33. Ray, T. R. et al. Soft, skin-interfaced sweat stickers for cystic fibrosis diagnosis and management. *Sci. Transl. Med.* **13**, eabd8109 (2021).
34. Lee, H. et al. A graphene-based electrochemical device with thermoresponsive microneedles for diabetes monitoring and therapy. *Nat. Nanotech.* **11**, 566–572 (2016).
35. Lee, H. et al. Wearable/disposable sweat-based glucose monitoring device with multistage transdermal drug delivery module. *Sci. Adv.* **3**, e1601314 (2017).
36. Kim, J. et al. Noninvasive alcohol monitoring using a wearable tattoo-based iontophoretic-biosensing system. *ACS Sens.* **1**, 1011–1019 (2016).
37. Kim, J. et al. A skin-interfaced, miniaturized microfluidic analysis and delivery system for colorimetric measurements of nutrients in sweat and supply of vitamins through the skin. *Adv. Sci.* **9**, 2103331 (2022).
38. Sempionatto, J. R. et al. Wearable and mobile sensors for personalized nutrition. *ACS Sens.* **6**, 1745–1760 (2021).
39. Yang, Y. et al. A laser-engraved wearable sensor for sensitive detection of uric acid and tyrosine in sweat. *Nat. Biotechnol.* **38**, 217–224 (2020).
40. Yu, Y. et al. Biofuel-powered soft electronic skin with multiplexed and wireless sensing for human-machine interfaces. *Sci. Robot.* **5**, eaaz7946 (2020).
41. Wang, J. Electrochemical biosensors: towards point-of-care cancer diagnostics. *Biosens. Bioelectron.* **21**, 1887–1892 (2006).
42. Uzun, L. & Turner, A. P. Molecularly-imprinted polymer sensors: realising their potential. *Biosens. Bioelectron.* **76**, 131–144 (2016).
43. Parlak, O., Keene, S. T., Marais, A., Curto, V. F. & Salleo, A. Molecularly selective nanoporous membrane-based wearable organic electrochemical device for noninvasive cortisol sensing. *Sci. Adv.* **4**, eaar2904 (2018).
44. Kaspar, H., Dettmer, K., Gronwald, W. & Oefner, P. J. Automated GC–MS analysis of free amino acids in biological fluids. *J. Chromatogr. B* **870**, 222–232 (2008).
45. Riedl, B., Nischik, M., Birklein, F., Neundörfer, B. & Handwerker, H. O. Spatial extension of sudomotor axon reflex sweating in human skin. *J. Auton. Nerv. Syst.* **69**, 83–88 (1998).
46. Newsholme, E. A. & Blomstrand, E. Branched-chain amino acids and central fatigue. *J. Nutr.* **136**, 274S–276S (2006).
47. Ahlqvist, E. et al. Novel subgroups of adult-onset diabetes and their association with outcomes: a data-driven cluster analysis of six variables. *Lancet Diabetes Endocrinol.* **6**, 361–369 (2018).
48. Layman, D. K. & Walker, D. A. Potential importance of leucine in treatment of obesity and the metabolic syndrome. *J. Nutr.* **136**, 319S–323S (2006).
49. Kitson, F. G., Larsen, B. S. & McEwen, C. N. *Mass Spectrometry: A Practical Guide*, pp. 3–23 (Academic Press, San Diego, 1996).
50. Torrente-Rodríguez, R. M. et al. Rapid endoglin determination in serum samples using an amperometric magneto-actuated disposable immunosensing platform. *J. Pharm. Biomed.* **129**, 288–293 (2016).

Acknowledgements

This project was supported by the National Institutes of Health grant R01HL155815, Office of Naval Research grants N00014-21-1-2483 and N00014-21-1-2845, the Translational Research Institute for Space Health through NASA NNX16AO69A, NASA Cooperative Agreement 80NSSC20M0167, High Impact Pilot Research Award T31IP1666 and grant R01RG3746 from the Tobacco-Related Disease Research Program, Caltech-City of Hope Biomedical Initiative Pilot Grant and the Rothenberg Innovation Initiative Program at California Institute of Technology. J.T. was supported by the National Science Scholarship (NSS) from the Agency of Science Technology and Research (A*STAR) Singapore. We gratefully acknowledge critical support and infrastructure provided for this work by the Kavli Nanoscience Institute at Caltech. This project benefitted from the use of instrumentation made available by the Caltech Environmental Analysis Center, and we gratefully acknowledge support on GC–MS from N. Dalleska. We also gratefully acknowledge Z. Wang for the contribution to mobile app development, R. M. Torrente-Rodríguez for the insulin assay optimization and S. Bao for the valuable inputs.

Author contributions

W.G., M.W., Y.Y. and J.M. initiated the concept and designed the studies; W.G. supervised the work; M.W., Y.Y. and J.M. led the experiments and collected the overall data; Y.S., J.T., D.M., C.Y. and C.X. contributed to sensor characterization, validation and sample analysis; N.H. contributed to the signal processing and app development. J.S.M., T.K.H. and Z.L. contributed to the design of the human studies. W.G., M.W., Y.Y. and J.M. co-wrote the paper. All authors contributed to the data analysis and provided feedback on the manuscript.

Competing interests

The authors declare no competing interests.

Additional information

Supplementary information The online version contains supplementary material available at https://doi.org/10.1038/s41551-022-00916-z.

Correspondence and requests for materials should be addressed to Wei Gao.

Peer review information *Nature Biomedical Engineering* thanks the anonymous reviewers for their contribution to the peer review of this work.

Reprints and permissions information is available at www.nature.com/reprints.

Publisher's note Springer Nature remains neutral with regard to jurisdictional claims in published maps and institutional affiliations.

nature research

Corresponding author(s): Wei Gao

Last updated by author(s): May 30, 2022

Reporting Summary

Nature Research wishes to improve the reproducibility of the work that we publish. This form provides structure for consistency and transparency in reporting. For further information on Nature Research policies, see our Editorial Policies and the Editorial Policy Checklist.

Statistics

For all statistical analyses, confirm that the following items are present in the figure legend, table legend, main text, or Methods section.

n/a	Confirmed	
☐	☒	The exact sample size (*n*) for each experimental group/condition, given as a discrete number and unit of measurement
☐	☒	A statement on whether measurements were taken from distinct samples or whether the same sample was measured repeatedly
☒	☐	The statistical test(s) used AND whether they are one- or two-sided *Only common tests should be described solely by name; describe more complex techniques in the Methods section.*
☒	☐	A description of all covariates tested
☒	☐	A description of any assumptions or corrections, such as tests of normality and adjustment for multiple comparisons
☐	☒	A full description of the statistical parameters including central tendency (e.g. means) or other basic estimates (e.g. regression coefficient) AND variation (e.g. standard deviation) or associated estimates of uncertainty (e.g. confidence intervals)
☒	☐	For null hypothesis testing, the test statistic (e.g. *F*, *t*, *r*) with confidence intervals, effect sizes, degrees of freedom and *P* value noted *Give P values as exact values whenever suitable.*
☒	☐	For Bayesian analysis, information on the choice of priors and Markov chain Monte Carlo settings
☒	☐	For hierarchical and complex designs, identification of the appropriate level for tests and full reporting of outcomes
☐	☒	Estimates of effect sizes (e.g. Cohen's *d*, Pearson's *r*), indicating how they were calculated

Our web collection on statistics for biologists contains articles on many of the points above.

Software and code

Policy information about availability of computer code

Data collection	Mbed was used to program the microcontroller. CH Instrument was used for off-body sensor data collection. Comsol was used for the simulations.
Data analysis	Origin 2018 was used to analyse and plot all the data, and to calculate the statistical parameters.

For manuscripts utilizing custom algorithms or software that are central to the research but not yet described in published literature, software must be made available to editors and reviewers. We strongly encourage code deposition in a community repository (e.g. GitHub). See the Nature Research guidelines for submitting code & software for further information.

Data

Policy information about availability of data

All manuscripts must include a data availability statement. This statement should provide the following information, where applicable:

- Accession codes, unique identifiers, or web links for publicly available datasets
- A list of figures that have associated raw data
- A description of any restrictions on data availability

The main data supporting the results in this study are available within the paper and its Supplementary Information. Source data for Figs. 4 and 5 and for Supplementary Figs. 36 and 39–41 are provided with this paper. All raw and analysed datasets generated during the study are available from the corresponding author on request.

Field-specific reporting

Please select the one below that is the best fit for your research. If you are not sure, read the appropriate sections before making your selection.

☒ Life sciences ☐ Behavioural & social sciences ☐ Ecological, evolutionary & environmental sciences

For a reference copy of the document with all sections, see nature.com/documents/nr-reporting-summary-flat.pdf

Life sciences study design

All studies must disclose on these points even when the disclosure is negative.

Sample size	For the on-body evaluation of the wearable sensor, 13 healthy subjects were recruited; for the sweat BCAA study, 10 normal-weight healthy subjects, 7 overweight or obese subjects, and 3 obese T2DM patients were involved; for COVID-19 metabolic fingerprint analysis, 8 COVID-19-positive and 8 COVID-19-negative samples were used. Sample sizes were chosen on the basis of standards in the literature for proof-of-concept experiments.
Data exclusions	No data were excluded.
Replication	All attempts at replication were successful when following the device-fabrication process described in the paper.
Randomization	The devices were fabricated with the same process and tested in all participants under same conditions. Randomization was therefore not relevant to the study.
Blinding	Blinding was not relevant, because a blinding process wouldn't influence the sampling result.

Reporting for specific materials, systems and methods

We require information from authors about some types of materials, experimental systems and methods used in many studies. Here, indicate whether each material, system or method listed is relevant to your study. If you are not sure if a list item applies to your research, read the appropriate section before selecting a response.

Materials & experimental systems

n/a	Involved in the study
☒	☐ Antibodies
☒	☐ Eukaryotic cell lines
☒	☐ Palaeontology and archaeology
☒	☐ Animals and other organisms
☐	☒ Human research participants
☒	☐ Clinical data
☒	☐ Dual use research of concern

Methods

n/a	Involved in the study
☒	☐ ChIP-seq
☒	☐ Flow cytometry
☒	☐ MRI-based neuroimaging

Human research participants

Policy information about studies involving human research participants

Population characteristics	Normal-weight healthy individuals with a body mass index (BMI) of 18.5 to 24.9 kg m-2 with fasting serum glucose < 100 mg dL-1 (Healthy); Overweight/obese individuals with a BMI of 25 to 35 kg m-2 and fasting serum glucose < 6 mg dL-1 (Overweight/Obesity); Obese individuals with a BMI of 25 to 35 kg m-2 and fasting serum glucose >= 126 mg dL-1 (Obesity & T2DM). COVID-19-positive and COVID-19-negative serum samples were purchased from RayBiotech, Inc.
Recruitment	The participating subjects were recruited from Caltech campus, UCLA hospital and the neighboring communities through advertisement by posted notices, word of mouth, and email distribution. There were no self-selection biases or other biases.
Ethics oversight	California Institute of Technology

Note that full information on the approval of the study protocol must also be provided in the manuscript.